Estimation of the entropy of the solar wind flow

Wiesław M. Macek* and Stefano Redaelli
Space Research Centre, Polish Academy of Sciences, Bartycka 18 A, 00-716 Warsaw, Poland
(Received 10 September 1999; revised manuscript received 27 July 2000)

We analyze a time series of velocities of the low-speed stream measured by the Helios spacecraft in the inner heliosphere, which is the region of space dominated by the solar wind flow. We use a nonlinear filter to give a faithful representation of the solar wind nonlinear behavior. We have demonstrated that the influence of noise in the data can be much more efficiently reduced by a nonlinear filter than with the conventional (linear) filters, and this allows a more realistic calculation of the solar wind entropy. The resulting Kolmogorov entropy is positive, and possibly the largest Lyapunov exponent is also positive locally, which would exhibit exponential sensitivity to initial conditions. Thus, these results show that the solar wind in the inner heliosphere is most likely a deterministic chaotic system.

PACS number(s): 05.45.Tp, 96.50.Ci, 95.10.Fh

I. INTRODUCTION

The dimensions of attractors and their entropies are important characteristics of dynamical systems. The Kolmogorov entropy is the rate of creation of information as a chaotic orbit evolves [1–3]. The entropy is equal to zero for a regular (periodic) system, a constant greater than zero for a chaotic deterministic system, and infinite for a stochastic random system; a positive and finite entropy implies chaos. However, both the dimension and entropy describe a kind of scaling behavior in the limit as the distances r between points on the attractor approach zero. These characteristics are sensitive to the presence of small amounts of noise, which may obscure the underlying fractal structure, unless the data are filtered to reduce noise contamination. In particular, a zero entropy or Lyapunov exponent can be driven positive by noise, or in the latter case just drift slightly positive as the exponent fluctuates near zero. Therefore, in order to detect and quantify chaos in any real dynamical system, it is necessary to deal with a cleaned experimental signal.

Following space physics applications, e.g., [4,5], we consider the inner heliosphere. Since the 1960s we have known that, besides electromagnetic radiation, the Sun also radiates charged particles, forming a plasma blowing nearly radially outward from the Sun. The solar wind plasma flowing supersonically away from the Sun is quite well modeled within the framework of hydromagnetic theory. This continuous flow has two forms: slow ($\approx$300 km s^{-1}) and fast ($\approx$900 km s^{-1}) [6]. The fast wind is associated with coronal holes and is relatively uniform and stable, while the slow wind is quite variable in terms of velocities. We limit our study to the low-speed stream. Indication for a chaotic attractor in the slow solar wind has recently been given in [7–10]. In particular, Macek [7] has provided tests for nonlinearity in the solar wind data, including a powerful method of singular-value decomposition [11] and statistical surrogate data tests [12].

In this paper we have extended our previous results on dimensional time series analysis [7], namely, we focus on the entropy of the solar wind. Therefore, we apply the modern technique of nonlinear noise reduction [13–15], which allows a more realistic calculation of the Kolmogorov entropy of the solar wind flow directly from the cleaned experimental signal by using the Grassberger and Procaccia method [16]. The data and importance of noise reduction are discussed in Sec. II. The method of estimation of the entropy and dimension is reviewed in Sec. III. Section IV is devoted to the main results of our calculations. In particular, we show that the correlation entropy of the attractor is positive and finite, as it should be for a chaotic system. The entropy is plausibly constrained by a positive local Lyapunov exponent that would exhibit sensitive dependence on initial conditions. In this way, we have further supported our previous conjecture that trajectories describing the system in the inertial manifold of phase space asymptotically approach the attractor of low dimension. These results provide some evidence that the complex solar wind is likely a deterministic chaotic system. One can also expect that this attractor should contain information about the dynamic variations of the coronal streamers. It is also possible that it represents a structure of the time sequence of near-Sun coronal fine-stream tubes; see [7] and references therein.

II. DATA AND NOISE

We analyze the Helios data using the radial velocity component v, measured in the heliosphere near the Sun [6]. We select an interval between the crossing of the interplanetary current sheet and the interplanetary shock. These raw data of $N=4514$ points are shown in [7, Fig. 1(a)]. As discussed in [7], slow trends ($349.7+21.74t-96.61t^2$, with t being a fraction of the total sample) were subtracted from the raw data and the resulting original data after detrending, $x_i = v(t_i)$, in km s^{-1}, $i=1,\ldots,N$, are now presented in Fig. 1(a). However, in [7] these data were eightfold smoothed (replacing each data point with the average of itself and its two nearest neighbors). Certainly, this is a particular linear finite impulse response (FIR) filter, which should preserve the correlation dimension [3]. On the other hand, in order to use filters correctly and to check their efficiency, it is impor-

*Fax: (4822) 840 3131. Email address: macek@cbk.waw.pl; http://www.cbk.waw.pl/~macek

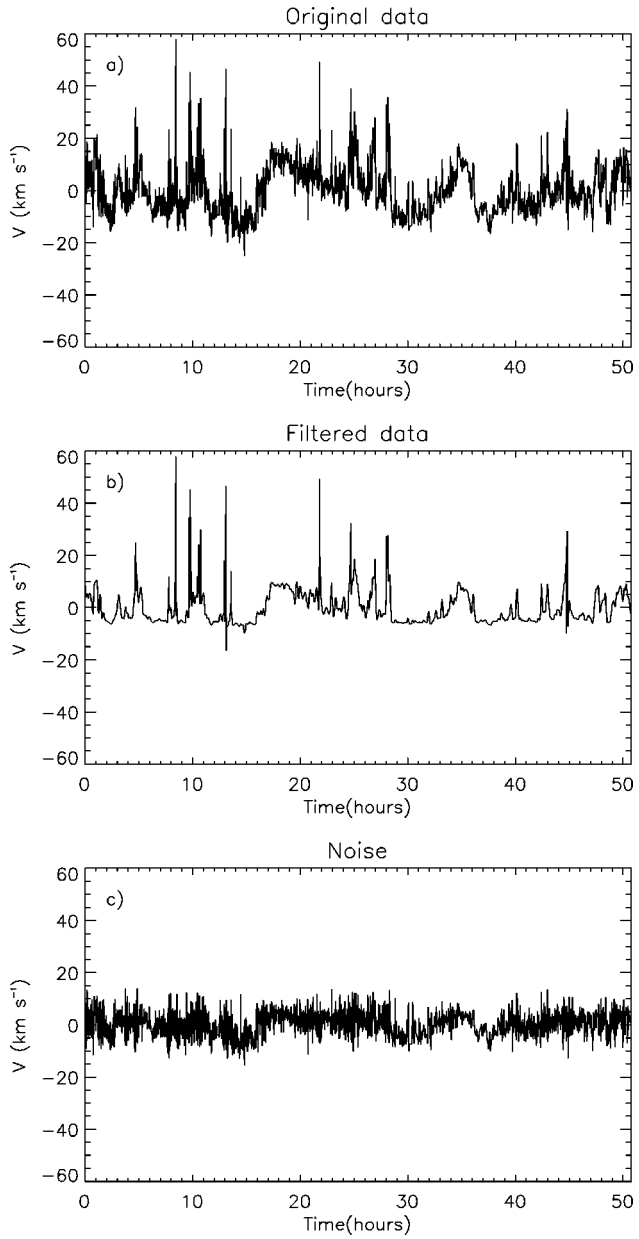

FIG. 1. The radial velocity v observed by the Helios 1 spacecraft in 1975 from 67:08:20.5 to 69:11:07 (day:h:min) at distances 0.32 AU from the Sun; (a) the original data, (b) the filtered data after nonlinear noise reduction, and (c) the noise removed by nonlinear filter.

tant to estimate the level of noise in the data before and after filtering. Therefore, we discuss the influence of noise reduction in detail as follows.

We assume that the data can be decomposed into two components, $x_i = y_i + \eta_i$, the clean signal with some noise added. The idea is to replace the measurement x_i, which contains noise, by a ''cleaned'' value x_i^{corr}. For example, in the case of the moving average FIR filter we have

$$x_i^{\mathrm{corr}} = \frac{1}{2l+1} \sum_{j=-l}^{l} x_{i+j}. \tag{1}$$

If the data are embedded in phase space of dimension m that is higher than that required to reconstruct the dynamics, k, the extra dimension is dominated by the noise, which results in a certain shape of the correlation sum as a function of distances r, and $D(k+1,r) = D(k,r) + d_{\mathrm{noise}}(r)$, where d_{noise} denotes the dimension of the distribution of noise. In general, we define the normalized effective dimension that is the signature of noise as

$$d_{m,k}(r) = \frac{D(m,r) - D(k,r)}{m-k}. \tag{2}$$

Assuming a Gaussian noise distribution we have the analytical formula [14]

$$d_{m,k}(r) = \frac{r e^{-(r/2\sigma)^2}}{\sigma \pi^{1/2} \mathrm{erf}(r/2\sigma)}. \tag{3}$$

The noise level σ may be determined by a simple fit, $\sigma^2 = \langle \eta^2 \rangle$. Although the noise does not seem to follow any Gaussian distribution, this simple formula can be used directly to estimate lower and upper bounds for the noise level as discussed in [15]. The normalized effective dimensions $d_{m,k}(r)$ given in Eq. (2) are shown in Fig. 2 for the following cases: (a) original data, (b) after the linear moving average filter, and (c) after nonlinear noise reduction. The solid lines denote lower and upper bounds for the estimated noise level. As seen from Fig. 2(a) the initial noise level is 4–6%. Certainly, the moving average filter removes some amount of noise. However, we have verified that after the moving average linear filter of Eq. (1) we still have a substantial amount of noise of 2–5% [see Fig. 2(b)]. In this case, even though the logarithm of the correlation sum in the scaling region can provide an estimation of the correlation dimension, the spacing between these functions for various embedding dimensions is not regular, preventing us from any reliable estimation of the entropy. Naturally, noise reduction is of more importance for estimating the entropy than for dimensions.

Therefore, in this paper, instead of using this linear filtering of the signal, we apply a nonlinear filter in order to reduce the noise more efficiently and to give a faithful representation of the nonlinear behavior of the solar wind. The nonlinear (Schreiber) filter works in embedding space of dimension $2l+1$ [13]. We construct embedding vectors that involve past and future coordinates $\mathbf{X}_i = (x_{i-l}, \ldots, x_{i+l})$, define a neighborhood of size ϵ, $|\mathbf{X}_i - \mathbf{X}_j| < \epsilon$, and then replace the data point by its mean value in the neighborhood,

$$x_i^{\mathrm{corr}} = \frac{1}{N_i} \sum_{|\mathbf{X}_i - \mathbf{X}_j| < \epsilon} x_j, \tag{4}$$

where N_i is the number of elements of the neighborhood [13].

In practice, we average over segments of the trajectory that are close for l time steps in the past and l in the future. The size of the neighborhood should be larger than the noise level assumed in the data. The procedure can be iterated by taking decreasing ϵ until no neighbors are found and no further correction is made (usually 2–3 iterations are enough). Summarizing, we use the Schreiber filter, which averages in the embedding space of a chosen dimension $2l+1$ and a defined neighborhood of size ϵ, about 2–3 times of the esti-

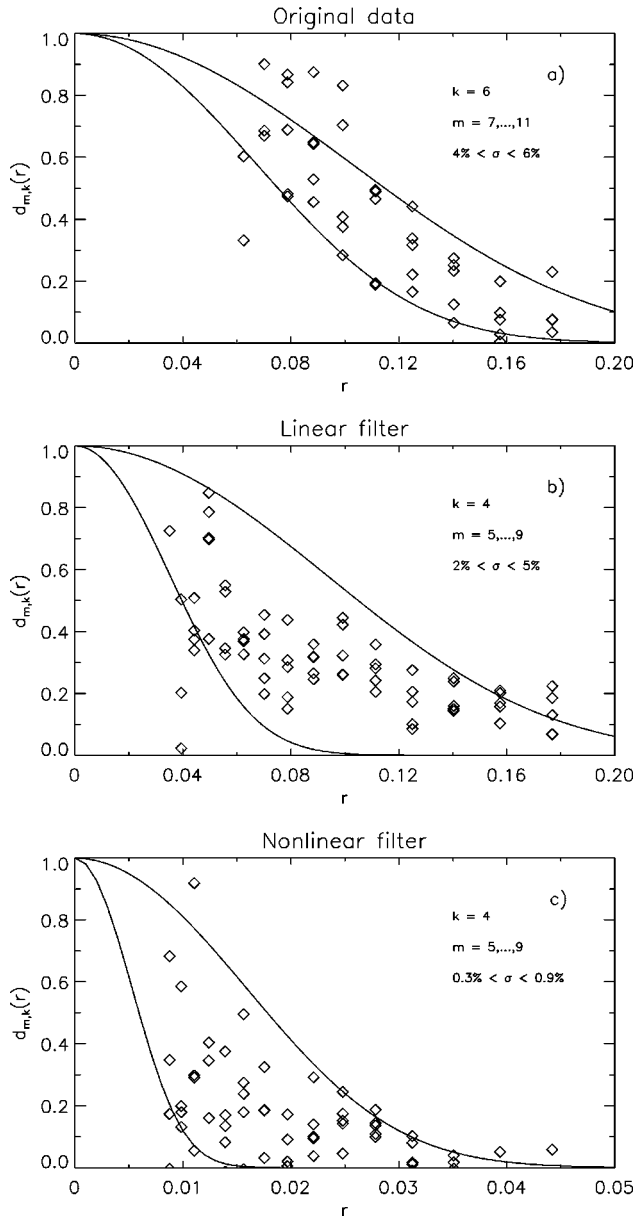

FIG. 2. The normalized effective dimension $d_{m,k}(r)$ given in Eq. (2), which is the signature of noise, as obtained for (a) original data, (b) data after linear moving average filter, and (c) data after nonlinear noise reduction. The solid lines denote lower and upper bounds for the estimated noise level. Only after nonlinear filtering has the noise been efficiently suppressed by half an order of magnitude, below 1%.

mated initial noise level [13]. We have performed three iterations taking the following input parameters: $l=3$, $\epsilon=0.15$; $l=6$, $\epsilon=0.08$; $l=6$, $\epsilon=0.012$. The filtered data after this procedure are shown in Fig. 1(b), and the noise [that is, the difference between the original data in Fig. 1(a) and the filtered data] is presented in Fig. 1(c). It is worth noting that only after nonlinear filtering has the noise efficiently been reduced to 0.3–0.9% [see Fig. 2(c)], i.e., by half an order of magnitude, as compared with the original data, Fig. 2(a). In addition, the calculated probability distribution of noise shown in Fig. 1(c) is roughly consistent with a normally distributed set of random numbers with $\sigma=0.05$. In this way, we have verified that by use of the nonlinear Schreiber filter

TABLE I. The solar wind velocity fluctuation data after nonlinear noise reduction.

Number of data points N	4514
Sampling time Δt	40.5 s
Skewness κ_3	1.88
Kurtosis κ_4	7.53
Relative complexity	0.12
Autocorrelation time t_a	1.6×10^3 s
Correlation dimension D_2[a]	2.7 ± 0.3
Entropy $(q=2)K_2$[b]	0.10 ± 0.06
Largest Lyapunov exponent λ_{max}[c]	~0.1
Predictability horizon time	$\sim10^4$ s

[a]The average slope for $6\leqslant m\leqslant10$ is taken as D_2.
[b]The average $(\Delta m=3)$ spacing between slopes for $8\leqslant m\leqslant12$ is taken as K_2.
[c]In the same units as K_2 (base e).

we have actually removed about 5% of the noise, leaving only a small non-Gaussian component (below 1%), as seen in Fig. 2(c).

Table I summarizes selected calculated characteristics of the detrended data cleaned by use of the Schreiber filter shown in Fig. 1(b). The probability distributions are non-Gaussian, more clearly than for the moving average filter, cf. Ref. [7]. We have a large skewness of 1.88 (as compared with its normal standard deviation of 0.06) and a very large kurtosis of 7.53 (the latter was small for the moving average filter). We have also estimated the Lempel-Ziv measure of complexity, relative to white noise [17]. The calculated value ~0.1 is even smaller than in [7] (~0.2); maximal complexity, or randomness, would have a value of 1.0, while a value of zero denotes perfect deterministic nonlinear predictability.

III. ENTROPY AND DIMENSION

As in [7], we choose a time delay $\tau=250\Delta t$ slightly larger than $t_0=212\Delta t$, the first zero of the autocorrelation function $(\langle v(t)v(t+t_0)\rangle-\langle v(t)\rangle^2)/\sigma^2=0$ with average velocity $\langle v\rangle=0.02\,\mathrm{km\,s^{-1}}$ and standard deviation $\sigma=8.07\,\mathrm{km\,s^{-1}}$, cf. also t_a in Table I when the autocorrelation function decreases by a factor $1/e$.

Using our time series of equally spaced, detrended, and cleaned data, we construct a large number of vectors $\mathbf{X}(t_i)=[v(t_i),v(t_i+\tau),\ldots,v(t_i+(m-1)\tau)]$ in the embedding phase space of dimension m, where $i=1,\ldots,n$ with $n=N-(m-1)\tau$. Then, we divide this space into a large number $M(r)$ of equal hypercubes of size r, which cover the presumed attractor. If p_j is the probability measure that a point from a time series falls in a typical jth hypercube, using the q-order function $I_q(r)=\Sigma(p_j)^q$, $j=1,\ldots,M$, the q-order Renyi-Kolmogorov information entropy is, e.g., [2,3,16],

$$K_q=\lim_{r\to0}\lim_{m\to\infty}\frac{1}{1-q}\ln I_q(r). \tag{5}$$

The related generalized dimension [2,3] is given by $D_q=[1/(q-1)]\lim_{r\to0}[\ln I_q(r)/\ln r]$, as has been discussed extensively in [7].

In practice, $q=2$ is sufficient and $I_2(r)$ is taken to be equal to the correlation sum [18]

$$C_m(r)=\frac{1}{n_{\mathrm{ref}}}\sum_{i=1}^{n_{\mathrm{ref}}}\frac{1}{n-2n_c-1}\sum_{j=n_c+1}^{n}\theta(r-|\mathbf{X}(t_i)-\mathbf{X}(t_j)|) \tag{6}$$

with $\theta(x)$ being the unit step function, where $n_{\mathrm{ref}}=500$ is the number of reference vectors and $n_c=4$ is Theiler's correction [19]. Since the correlation sum is simply an arithmetic average over the numbers of neighbors, this can yield meaningful results for the dimension and entropy even when the number of neighbors available for some reference points is limited in most real dynamical systems. For large m and small r in the scaling region it can be argued that

$$C_m(r)\propto r^{D_2}e^{-mK_2} \tag{7}$$

where D_2 and K_2 are approximations of the ideal $r\to 0$ and $m\to\infty$ limits in Eq. (5) for $q=2$ [16].

IV. RESULTS AND DISCUSSION

In Figs. 3–6 we show the results of our calculations as obtained for the following data sets: (a) the original data, (b) the cleaned experimental signal after nonlinear noise reduction, and (c) the noise that has been removed by the nonlinear filter. First, we calculate the natural logarithm of the correlation sum $C_m(r)$ versus $\ln r$ (normalized) for various embedding dimensions: $m=4$ (dotted curve), 5 (diamonds), 6 (triangles), 7 (squares), 8 (crosses), and 9 (plus signs). The results obtained using the nonlinear Schreiber filter are presented in Fig. 3(b), while those obtained using the moving average and singular-value decomposition linear filters have been discussed extensively in [7].

The slopes $D_{2,m}(r)=d[\ln C_m(r)]/d(\ln r)$ of the correlation sum $C_m(r)$ versus $\ln r$ obtained for various embedding dimensions m for (a) original data, (b) after nonlinear noise reduction, and (c) noise removed by nonlinear filter are shown in Figs. 4(a)–4(c). As discussed in [14], usually one can distinguish different types of behavior of $D_{2,m}(r)$ for different regions of scale r. Obviously, for very small r the lack of points is the dominant feature resulting in large statistical fluctuations. Somewhat larger r are dominated by the noise in the data and in this case we expect that $D_{2,m}(r)$ should be proportional to the embedding dimension m. Farther, in the proper scaling region of distances r, if the D-dimensional attractor exists, we expect a plateau of the slopes for $m\geqslant D$ [20] and in the worst case for $m>2D$ [21]; the plateau independent of m should provide the proper correlated dimension. Naturally, if distances r are of the order of the size of the entire attractor, scale invariance is no longer expected.

For the case of the moving average and singular-value decomposition linear filters the range of r with the meaningful plateau of slopes is limited to $-3.0<\ln r<-1.5$ (see [7]). The slopes obtained by using the nonlinear Schreiber filter are shown in Fig. 4(b). Here, using the Schreiber filter, owing to more efficient noise reduction for small distances, the plateau is obtained for $-4.5<\ln r<-2.0$. Comparison of this plateau for dimension after nonlinear noise reduction, Fig. 4(b), with the corresponding plateau after using the linear moving average filter [7, Fig. 7(a)] shows that the former is wider, clearer, and shifted toward smaller distances, but the slopes are somewhat smaller. Further, its width agrees with the estimates given by Olbrich and Kantz in [22]. They have shown that on large scales the data cannot be distinguished from random data and the determinism becomes visible only below a certain length scale. Therefore the plateau in Fig. 4(b) ends at about $r\sim e^{-2}$.

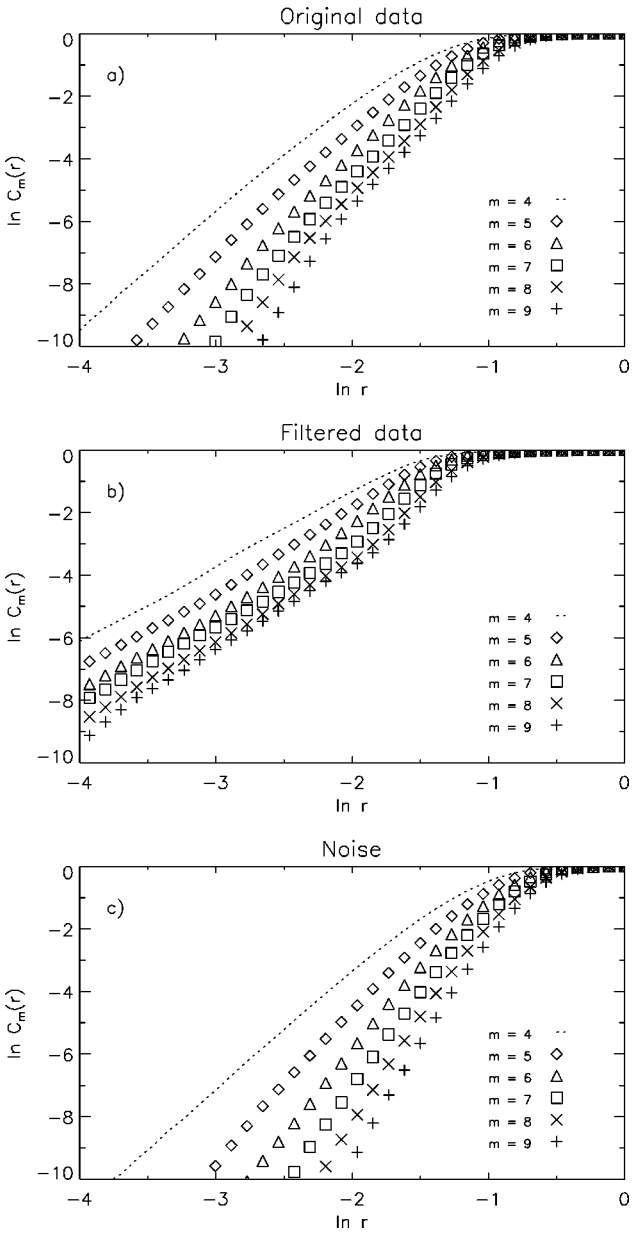

FIG. 3. The natural logarithms of the correlation sum $C_m(r)$ versus $\ln r$ (normalized) are shown for various embedding dimensions $m=4$ (dotted curve), 5 (diamonds), 6 (triangles), 7 (squares), 8 (crosses), and 9 (plus signs) as obtained for (a) original data, (b) data after nonlinear noise reduction, and (c) noise removed by nonlinear filter.

For m large enough an average slope in the scaling region indicates a proper correlation dimension D_2. In Fig. 4(b) we see a clear plateau, which appears already for $m=4$ (dotted curve) and $m=5$. For higher dimensions, $m\geqslant 10$, the plateau is still present but more smeared out by the statistical fluctuations at small r. In the case of the moving average filter,

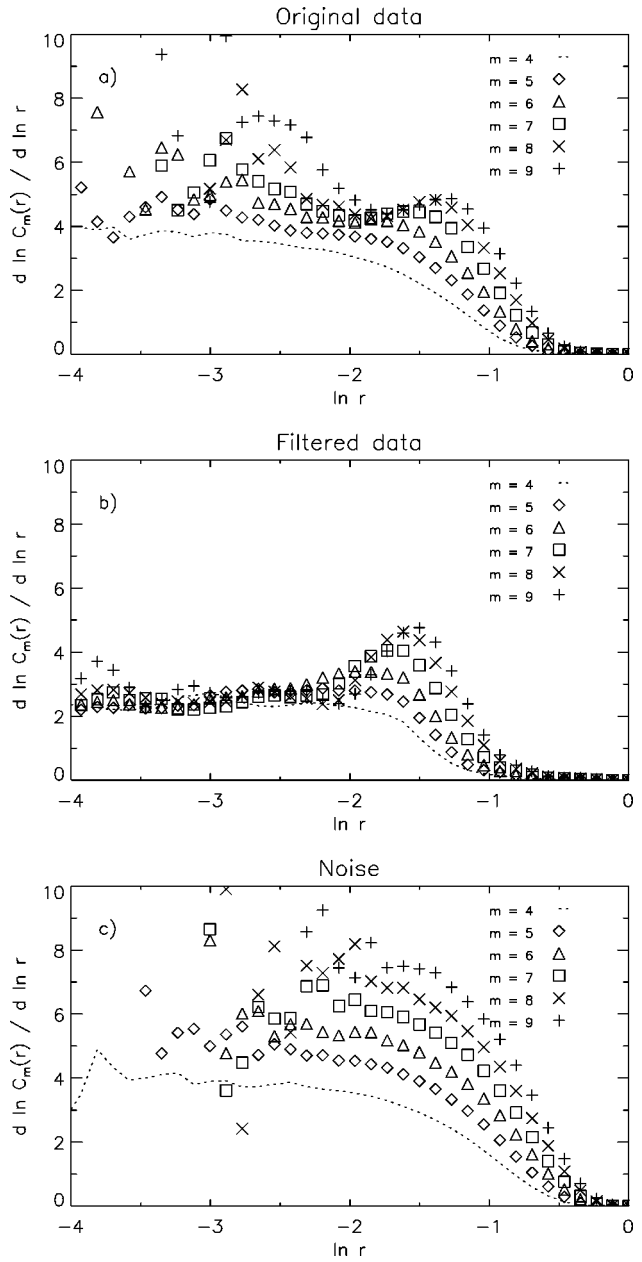

FIG. 4. The slopes $D_{2,m}(r)=d[\ln C_m(r)]/d(\ln r)$ of the correlation sum $C_m(r)$ versus $\ln r$ obtained for (a) original data, (b) data after nonlinear noise reduction, and (c) noise removed by nonlinear filter shown for various embedding dimensions m.

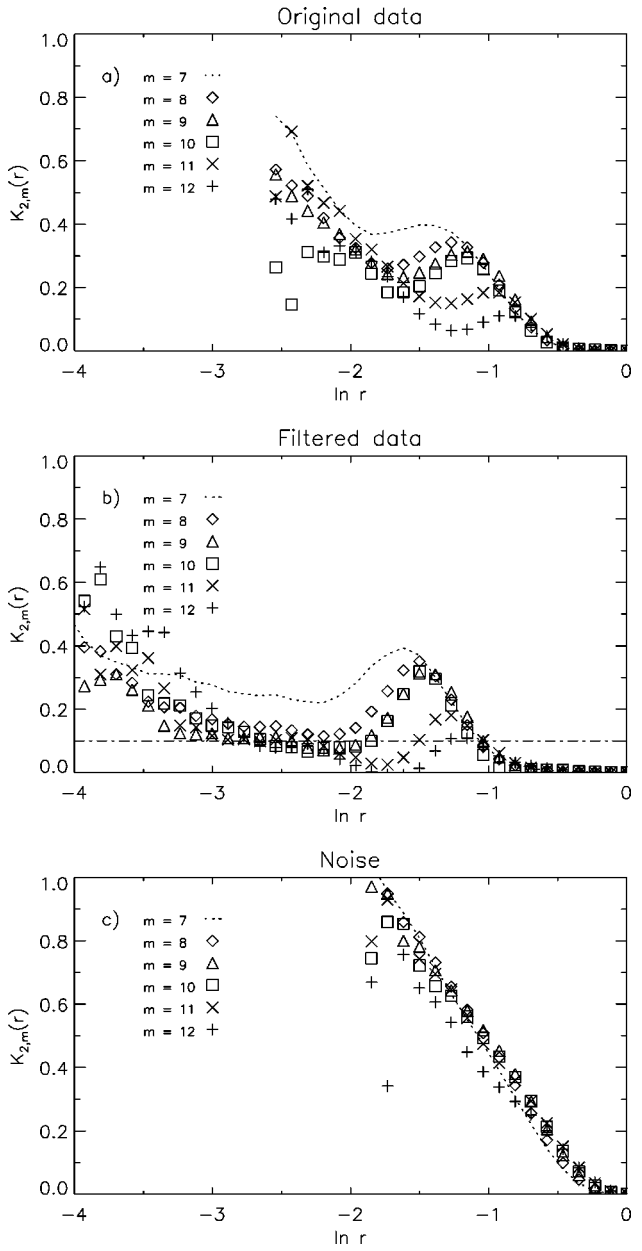

FIG. 5. The function $K_{2,m}(r)=(1/\Delta m)\ln[C_m(r)/C_{m+\Delta m}(r)]$ versus $\ln r$ ($\Delta m=3$) for various embedding dimensions m calculated for (a) original data, (b) cleaned experimental signal after nonlinear noise reduction, and (c) noise removed by nonlinear filter. Only in case (b) is there a clear plateau at $K_2\approx 0.1$ (base e), dash-dotted line.

the slope of the calculated correlation sum saturates for $m>5$, with an average for $6\leqslant m\leqslant 10$ providing $D_2=3.7\pm 0.3$ (see Ref. [7]); this is consistent with the attractor of low dimension. Now, as seen from Fig. 4(b), the corresponding average slope for the Schreiber filter is considerably smaller, $D_2=2.7\pm 0.3$. Admittedly, filtering can, in general, change the dimension of the attractor. It can be proved that every generic finite-step moving average filter preserves the correlation dimension, because it preserve the one-to-one property [3]. On the other hand, infinite impulse response filters may only increase the dimension [23], which is equivalent to augmenting the system with a new variable [3]. Conversely, we see that after the nonlinear Schreiber filter the calculated dimension has been somewhat reduced.

Second, for a given Δm, the average vertical spacing between the straight lines in Fig. 3,

$$K_{2,m}(r)=\frac{1}{\Delta m}\ln\frac{C_m(r)}{C_{m+\Delta m}(r)}, \tag{8}$$

is related to the correlation entropy (second order, $q=2$) [18]. Namely, for values of r inside the plateau in the dimension plots the factor r^{D_2} in Eq. (7) is almost constant and we can determine the entropy by plotting $K_{2,m}(r)$ both versus r for various m, Fig. 5, and versus m for various r, Fig. 6, again as calculated for the following data sets: (a) original

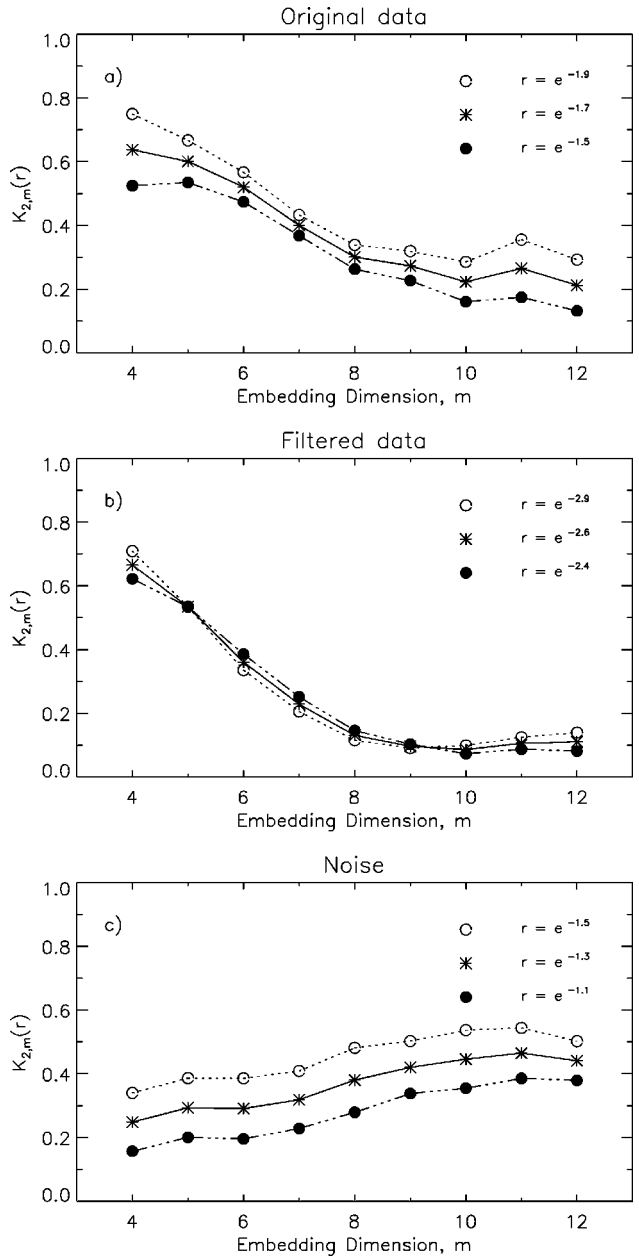

FIG. 6. The function $K_{2,m}(r)$ (base e) versus the embedding dimension m for various distances r in the scaling region calculated for (a) original data, (b) cleaned experimental signal after nonlinear noise reduction, and (c) noise removed by nonlinear filter. Only in case (b) does the average saturated value yield the correlation entropy of $K_2 = 0.10 \pm 0.06$; see Tables I and II.

data, (b) cleaned experimental signal after nonlinear noise reduction, and (c) noise that has been removed by the nonlinear filter.

The values of this function $K_{2,m}(r)$ given in Eq. (8) obtained after noise reduction versus $\ln r$ are shown in Fig. 5(b) for various embedding dimensions m (we take $\Delta m = 3$). For $8 \leqslant m \leqslant 12$ there is a plateau at $K_2 \approx 0.1$ (base e) (dash-dotted line). Strictly speaking, the ideal entropy of Eq. (5) is defined in the $m \to \infty$ limit (in addition to the $r \to 0$ limit for both the dimension and entropy). However, the available number of vectors decreases with m and the higher dimensions are dominated by noise, as discussed in Secs. II and III. Admittedly, it is not surprising that the plateau of $K_{2,m}(r)$ in Fig. 5(b) for the entropy is narrower than the plateau for $D_{2,m}(r)$ in Fig. 4(b) for the dimension. Apparently, these plateaus are also limited for large r, especially for large m, as seen for $m = 11$ and 12 in Fig. 5(b) (a large number of points is needed for $m > 10$). Nevertheless, as discussed in [22], we can calculate the entropy below a length scale of $r \sim e^{-2}$. In contrast, there is no plateau even for moderate m for the original data contaminated with noise, Fig. 5(a), and, obviously, for any m for the noise itself, Fig. 5(c). As seen in Fig. 3(c), the correlation sums are converging with $\ln r$. Hence the spacing between the lines in Eq. (8) is decreasing linearly with $\ln r$, as shown in Fig. 5(c), which is a typical behavior for the noise case. On the other hand, for an ideal deterministic system, for large m within a scaling region, the spacing between the parallel straight lines should be constant. This demonstrates that the modern technique of nonlinear noise reduction [13–15] is necessary for a realistic calculation of the Kolmogorov entropy in the solar wind flow, and probably in most real complex systems. By the way, the plateau in Fig. 5(b) for the cleaned solar wind data is similar to the plateau for the (nuclear magnetic resonance) laser data (with a larger number of data points, $N = 38\,000$) obtained after nonlinear noise reduction by Kantz and Schreiber, cf. ([15], Fig. 11.3).

TABLE II. The correlation entropy $K_2(r)$ calculated from the cleaned experimental data.

$\ln r$	Average $8 \leqslant m \leqslant 12$
-2.4	0.10 ± 0.03
-2.5	0.10 ± 0.04
-2.6	0.10 ± 0.06
-2.8	0.11 ± 0.07
-2.9	0.11 ± 0.08
Average over $\ln r$	0.10 ± 0.06

Next, the vertical spacing between the straight lines $K_{2,m}(r)$ calculated using the nonlinear filter versus the embedding dimension m (for $m = 4, \ldots, 12$) for various distances r in the scaling region with a plateau is shown in Fig. 6 for (a) original data, (b) filtered data, and (c) noise. In the ideal case (infinite number of data points) the entropy for noise would increase to infinity with increasing m, and in particular we would have a linear increase for a Gaussian noise. Conversely, the entropy should decrease to zero for a regular periodic system and to a constant greater than zero for a deterministic aperiodic system. Again, only for the filtered data in Fig. 6(b) do we see a clear saturation, while for the case of noise, Fig. 6(c), the calculated entropy increases with m, as it should for a stochastic system. Naturally, as for any real system, because the number of available vectors is decreasing with m, the entropy for the noise removed from the solar wind data ceases to increase in Fig. 6(c).

We also calculate the largest positive Lyapunov exponent $\lambda_{\max}$ using a quite robust algorithm of Kantz [24]. We obtain the magnitude of ~ 0.1 for the data after nonlinear noise reduction, in the same units as for K_2 (base e). Certainly, a reliable calculation of the Lyapunov exponent would require many more data points. Therefore, we can only demonstrate that a positive largest Lyapunov exponent is not excluded. In

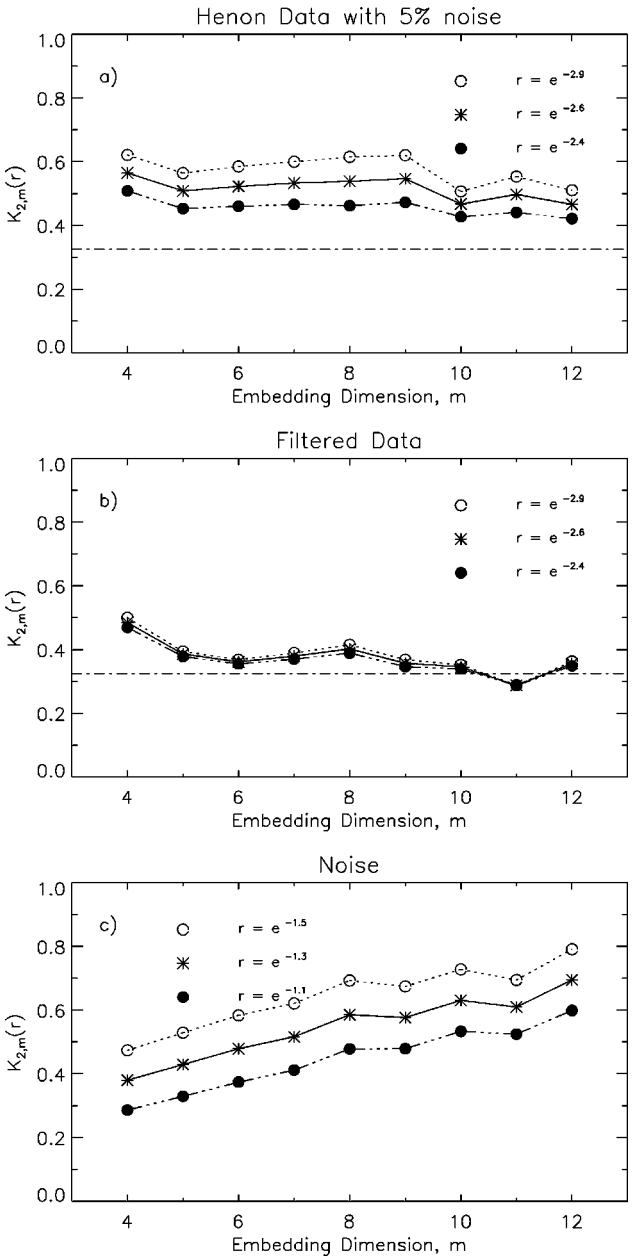

FIG. 7. The function $K_{2,m}(r)$ (base e) versus the embedding dimension m for various distances r in the scaling region calculated for the Hénon map ($a=1.4$, $b=0.3$) using 2000 iterates for (a) data file with 5% noise, (b) filtered data after nonlinear noise reduction, and (c) noise removed by nonlinear filter. Only in case (b) does the average saturated value yield the proper correlation entropy of $K_2=0.325$ (dash-dotted line).

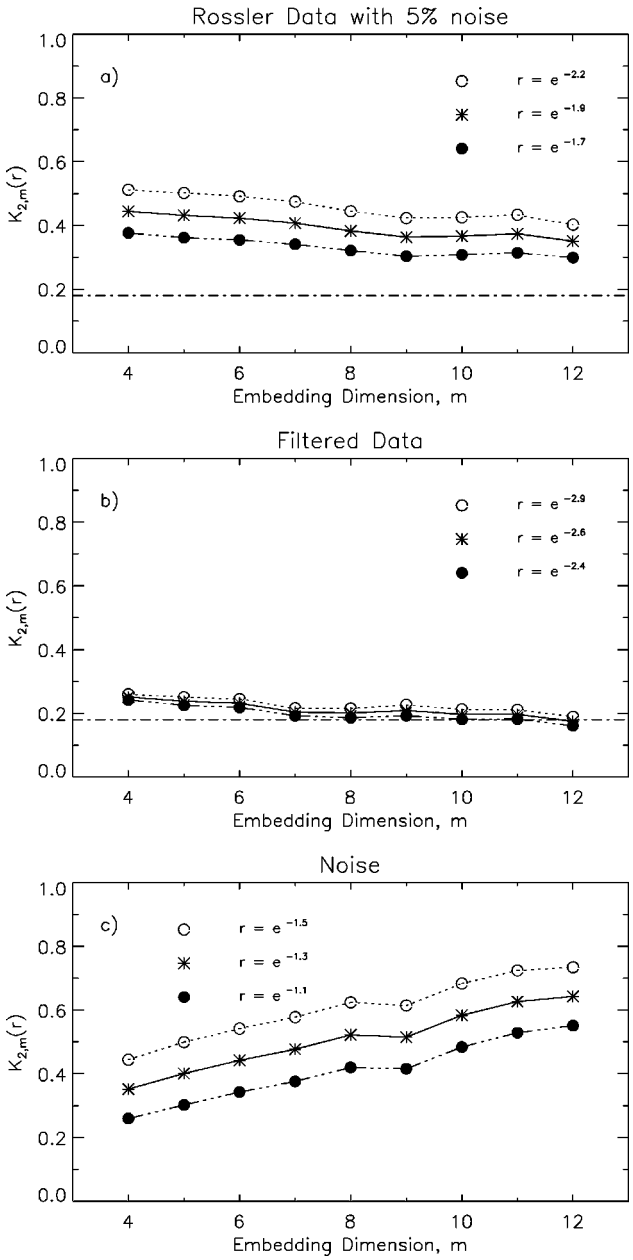

FIG. 8. The function $K_{2,m}(r)$ (base e) versus the embedding dimension m for various distances r in the scaling region calculated for Rössler chaos equations ($a=0.15$, $b=0.2$, $c=10$) using 4096 data points at intervals of $\Delta t=0.3$ s, $\tau=2\Delta t$; (a) data file with 5% noise, (b) filtered data after nonlinear noise reduction, and (c) noise removed by nonlinear filter.

general, the entropy K_q is at most the sum of the positive Lyapunov exponents $\Sigma\lambda_i$, e.g., [3]. As shown in Table I, the value of the Lyapunov exponent is consistent with the correlation entropy $K_2=0.1$, which should be its lower bound: $K_2 \leqslant \Sigma\lambda_i$ (positive). The time over which the meaningful prediction of the behavior of the system is possible is roughly $\sim 1/\lambda_{\max}$, e.g., [3]. Hence the predictability of the system would be limited to hours [10].

The measures of the attractor obtained have also been subjected to surrogate data tests [12]. As is shown in [7], Fig. 8, if the original data are indeed deterministic, analysis of these surrogate data will provide values that are statistically distinct from those derived for the original data. Again, we have found here that the solar wind data are sensitive to this test. In particular, as compared with the values of Table I, the Lempel-Ziv complexity calculated for shuffled data becomes 1.0. Further, contrary to the case of the filtered solar wind data, there is no saturation of the function $K_{2,m}(r)$ for the surrogate data for large m; instead this function increases with m as it should for stochastic data.

Our next point is comparison of the estimates of the solar wind entropy with other classical model systems corrupted by noise. Therefore, we have rerun our analysis also with two typical model systems: a discrete chaotic Hénon map, which is often used for calibration of the largest Lyapunov

exponent ($a=1.4$, $b=0.3$) using 2000 iterates, and a continuous chaotic system generated by Rössler equations ($a=0.15$, $b=0.2$, $c=10$) using 4096 data points at intervals of $\Delta t=0.3$ s, $\tau=2\Delta t$, both with purposely added 5% noise. The calculated values of $K_{2,m}(r)$ for both cases using the nonlinear Schreiber filter versus the embedding dimension m (for $m=4,\ldots,12$) for various distances r in the scaling region with a plateau for (a) data file with added 5% noise, (b) filtered data, and (c) noise removed by nonlinear filter are shown in Figs. 7 and 8, respectively. Only for the filtered data files (b) does the average saturated value yield the proper correlation entropy (dash-dotted lines), e.g., $K_2=0.325\pm0.02$ in Fig. 7(b) for the Hénon map [16]. Since the number of available vectors is decreasing with m, the entropy for the noise removed from the initially noisy Hénon map in Fig. 7(c) and for the noise removed by nonlinear filter from the noisy Rössler data in Fig. 8(c) ceases to increase with m. A somewhat similar saturation for large m is also seen in Fig. 6(c) for the solar wind data. Also, deviations from linear increase are seen in all these figures, Figs. 6(c), 7(c), and 8(c), because the Schreiber filter does not necessarily remove only a Gaussian noise, but possibly also its non-Gaussian component. On the other hand, in the corresponding case of the data cleaned by nonlinear filter in Figs. 6(b), 7(b), and 8(b) the entropy is decreasing with m, finally saturating for large m. Clearly, the saturation in these figures cannot result from decreasing of the available number of vectors with m, because, just on the contrary, we would rather have had a deeper decrease of K_2 with m instead. Hence we believe that the saturation results from a deterministic component of the system dynamics. Therefore, an artifact in saturation in Fig. 6(b) is highly improbable. Surprisingly, the saturation for the solar wind data is even better than the saturation for the well-known noisy Rössler system, with roughly the same number of points as our complex solar wind system, and for the classical noisy Hénon map, but with a smaller number of points (both cleaned by nonlinear filter). This shows again that the saturation in Fig. 6(b) for the solar wind is not artificial. We have verified the robustness of the main results against change in both parameters r and m. Thus, we can expect that for sufficiently large m in the scaling region K_2 should converge toward a constant according to Eq. (7). Admittedly, this is merely an approximation of the ideal $m\to\infty$ limit in Eq. (5) for $q=2$.

Finally, the spacings between the parallel lines averaged in the saturation region $8\leqslant m\leqslant 12$ are taken as $K_2(r)$. These saturated values given in Fig. 6(b) averaged over $\ln r$ yield the correlation entropy $K_2=0.10\pm0.06$ (base e). Naturally, the errors given in Tables I and II are obtained assuming their normal distribution over the scaling range. Certainly, these errors increase for smaller r and the maximum error in the scaling region is given here. Anyway, a clear saturation of $K_{2,m}(r)$ in Fig. 6(b) for $8\leqslant m\leqslant 12$ and various r in the scaling region, below a critical scale of $r\sim e^{-2}$, shows that the correlation entropy of the attractor is positive and finite, as it should be for a chaotic system.

V. CONCLUSIONS

To conclude, the moving average linear filter removes some amount of noise (leaving several percent). However, in practice, it could also possibly increase the calculated correlation dimension. In contrast, after the nonlinear Schreiber filter, owing to more efficient noise reduction at small distances, we have obtained a better plateau, which is wider and shifted toward smaller distances, but the dimension is somewhat reduced. However, this technique of nonlinear noise reduction allows a more realistic estimation of the Kolmogorov correlation entropy. The entropy is positive, and plausibly the largest Lyapunov exponent is also positive locally, which would exhibit sensitive dependence on initial conditions. The characteristics of the attractor obtained are significantly different from those of the surrogate data. Hence we suggest that there exists an inertial manifold for the solar wind in the inner heliosphere, in which the system is nonlinear and possibly chaotic, and where noise is certainly not dominant. This means that the observed irregular behavior of the velocity fluctuations results from intrinsic nonlinear chaotic dynamics rather than from random external forces.

ACKNOWLEDGMENT

This work was supported by the State Scientific Research Committee through Grant No. 2 P03C 001 16.

[1] H. G. Schuster, *Deterministic Chaos* (VCH, Weinheim, Germany, 1989).
[2] E. Ott, *Chaos in Dynamical Systems* (Cambridge University Press, Cambridge, England, 1993).
[3] E. Ott, T. Sauer, and J. A. Yorke, *Coping with Chaos* (Wiley, New York, 1994).
[4] J. Kurths and H. Herzel, Physica D **25**, 165 (1987).
[5] V. Carbone, P. Veltri, and R. Bruno, Phys. Rev. Lett. **75**, 3110 (1995).
[6] R. Schwenn, in *Physics of the Inner Heliosphere*, edited by R. Schwenn and E. Marsch (Springer-Verlag, Berlin, 1990), Vol. 20, pp. 99–182.
[7] W. M. Macek, Physica D **122**, 254 (1998).
[8] W. M. Macek, in *Solar Wind Nine*, edited by S. R. Habbal, R. Esser, J. V. Hollweg, and P. A. Isenberg (American Institute of Physics, New York, 1999) Vol. 471, pp. 251–254.
[9] W. M. Macek and L. Obojska, in *Environment Modelling for Space-based Applications, SP-392*, edited by A. Hilgers and T.-D. Guyenne (ESTEC, Noordwijk, 1996), pp. 247–252.
[10] W. M. Macek and L. Obojska, Chaos, Solitons Fractals **8**, 1601 (1997); **9**, 221 (1998).
[11] A. M. Albano, J. Muench, C. Schwartz, A. I. Mess, and P. E. Rapp, Phys. Rev. A **38**, 3017 (1988).
[12] J. Theiler, S. Eubank, A. Longtin, B. Galdrikian, and J. D. Farmer, Physica D **58**, 77 (1992).
[13] T. Schreiber, Phys. Rev. E **47**, 2401 (1993).
[14] T. Schreiber, Phys. Rev. E **48**, R13 (1993).
[15] H. Kantz and T. Schreiber, *Nonlinear Time Series Analysis* (Cambridge University Press, Cambridge, 1997).
[16] P. Grassberger and I. Procaccia, Phys. Rev. A **28**, 2591 (1983).

[17] F. Kaspar and H. G. Schuster, Phys. Rev. A **36**, 842 (1987).
[18] P. Grassberger and I. Procaccia, Physica D **9**, 189 (1983).
[19] J. Theiler, Phys. Rev. A **34**, 2427 (1986).
[20] M. Ding, C. Grebogi, E. Ott, T. Sauer, and J. A. Yorke, Phys. Rev. Lett. **70**, 3872 (1993).
[21] F. Takens, in *Dynamical Systems and Turbulence*, edited by D. A. Rand and L. S. Young, Lecture Notes in Mathematics Vol. 898 (Springer-Verlag, Berlin, 1981), pp. 366–381.
[22] E. Olbrich and H. Kantz, Phys. Lett. A **232**, 63 (1997).
[23] R. Badii, G. Broggi, B. Derighetti, M. Ravani, S. Ciliberto, A. Politi, and M. A. Rubio, Phys. Rev. Lett. **60**, 979 (1988).
[24] H. Kantz, Phys. Lett. A **185**, 77 (1994).